

Communication

Forbidden Coherence Transfer of ^{19}F Nuclei to Quantitatively Measure the Dynamics of a CF_3 -Containing Ligand in Receptor-Bound States

Yuji Tokunaga ¹, Koh Takeuchi ¹ and Ichio Shimada ^{1,2,*}

¹ Molecular Profiling Research Center for Drug Discovery, National Institute of Advanced Industrial Science and Technology (AIST), 2-3-26 Aomi, Koto-ku, Tokyo 135-0064, Japan; tokunaga.y@aist.go.jp (Y.T.); koh-takeuchi@aist.go.jp (K.T.)

² Graduate School of Pharmaceutical Sciences, the University of Tokyo, 7-3-1 Hongo, Bunkyo-ku, Tokyo 113-0033, Japan

* Correspondence: shimada@iw-nmr.f.u-tokyo.ac.jp; Tel.: +81-3-3815-6540

Received: 10 August 2017; Accepted: 4 September 2017; Published: 7 September 2017

Abstract: The dynamic property of a ligand in the receptor-bound state is an important metric to characterize the interactions in the ligand–receptor interface, and the development of an experimental strategy to quantify the amplitude of motions in the bound state is of importance to introduce the dynamic aspect into structure-guided drug development (SGDD). Fluorine modifications are frequently introduced at the hit-to-lead optimization stage to enhance the binding potency and other characteristics of a ligand. However, the effects of fluorine modifications are generally difficult to predict, owing to the pleiotropic nature of the interactions. In this study, we report an NMR-based approach to experimentally evaluate the local dynamics of trifluoromethyl (CF_3)-containing ligands in the receptor-bound states. For this purpose, the forbidden coherence transfer (FCT) analysis, which has been used to study the dynamics of methyl moieties in proteins, was extended to the ^{19}F nuclei of CF_3 -containing ligands. By applying this CF_3 -FCT analysis to a model interaction system consisting of a ligand, AST-487, and a receptor, p38 α , we successfully quantified the amplitude of the CF_3 dynamics in the p38 α -bound state. The strategy would bring the CF_3 -containing ligands within the scope of dynamic SGDD to improve the affinity and specificity for the drug-target receptors.

Keywords: NMR spectroscopy; dynamics; structural biology; drug development; trifluoromethyl

1. Introduction

The affinity and specificity of small molecules to their targets need to be improved in the hit-to-lead and the lead optimization processes in drug development. Target specificity is known to be associated with the thermodynamic properties of binding [1]. Ligands with larger enthalpic contributions to the receptor-binding free energy are expected to show better target specificity and to be less susceptible to drug-resistance mutations [2–4]. Such enthalpy-driven bindings are usually derived from multiple site-specific intermolecular interactions, such as hydrogen bonds and van der Waals interactions. The static structures of ligand–receptor complexes, mainly provided by X-ray crystallography, are able to identify those intermolecular interactions. However, the energetic contribution of each interaction cannot be readily predicted from a static structure. In this regard, the mobility of atoms in and near the intermolecular interaction site is expected to reflect the rigidity and strength of the local interaction [5–7]. Therefore, the current structure-guided drug development (SGDD) approaches, which rely largely on static structures, would be improved by taking the dynamic aspects of interactions into account and by developing experimental strategies to quantify the amplitude of motions.

Solution nuclear magnetic resonance (NMR) techniques have greatly contributed to pharmaceutical development at various stages [8–10]. NMR plays a critical role in the supply of intermolecular distance

information about ligand–receptor complexes, especially for the cases where solving the crystal structures of complexes is difficult. More importantly, the solution NMR techniques also provide information about the dynamics of both the ligands and the target biomolecules at an atomic resolution, with timescales ranging from picosecond to hour [11–16]. Among them, the forbidden coherence transfer (FCT) analyses have been established to quantify the amplitude of the ps–ns timescale motion of methyl (CH₃) groups in macromolecules [17]. The CH₃–FCT analyses extract two relaxation parameters: the intramethyl ¹H–¹H dipolar cross-correlated relaxation rate, η , and the sum of the dipolar cross-relaxation rates with external protons, δ . The parameter η is directly proportional to the generalized order parameter, S_{axis}^2 , which reports the amplitude of motion of the methyl threefold axis. The parameter δ is sensitive to the presence of remote protons within 3 Å, thus providing information about the surface complementarity if used in a ligand–receptor complex [18]. The advantages of the CH₃–FCT approach in ligand optimization were exemplified in our preceding research [18]. Here, the CH₃–FCT analyses were applied to a μM -affinity peptide ligand that binds to a drug-target kinase, to identify the methyl-bearing residues with a large motional amplitude and low surface complementarity in the kinase-bound state. The substitution of the residue with such propensities by a bulkier amino acid substantially improved the affinity and thermodynamic properties of the ligand.

Here, we report the extension of the FCT analysis to trifluoromethyl (CF₃) groups. Approximately 25% of therapeutic drugs on the market contain at least one fluorine atom, and the CF₃ group is one of the major fluorine-containing substituents [19]. Since recent advances in medicinal chemistry allow easy incorporation of fluorine atoms to specific sites of compounds [20,21], fluorine is frequently introduced at the lead optimization stage to enhance binding potency, oral availability, and/or metabolic stability [22,23]. The enhancement of the binding potency can be primarily attributed to the fluorine-mediated intermolecular interactions, including hydrogen bonds, halogen bonds, and van der Waals interactions. However, the strong electron-withdrawing propensity of fluorine also affects the interactions of remote functional groups, and the bulky fluorine substituent often modulates the dynamics of ligands in both the free and bound states. Such a pleiotropic nature makes the effects of fluorine incorporation difficult to predict. Therefore, implementation of a novel experimental approach to characterize the interaction and dynamics of compounds at fluorinated sites is of importance. As ¹⁹F is the 100% naturally abundant $\frac{1}{2}$ -spin nucleus with the next largest gyromagnetic ratio to the proton, it is feasible for use in NMR applications, and affords high sensitivity. In addition, the analysis of ¹⁹F-NMR spectra is straightforward, owing to the large chemical shift distribution (~100 ppm) and no background signals. These features make ¹⁹F-NMR an attractive approach in drug discovery [24], and the CF₃ moiety has been extensively used in drug-screening procedures due to its high sensitivity and relatively narrow line width [25,26].

In this report, we developed the CF₃–FCT analysis to quantitatively measure the dynamics of a CF₃-containing ligand in the receptor-bound state. The characteristics of the CF₃ groups that are distinct from those of the CH₃ groups—including the smaller gyromagnetic ratio, the longer spin–spin and van der Waals contact distances and the shorter ¹⁹F transverse relaxation times—were considered. We applied the strategy to a ligand, AST-487, complexed with a drug-target protein kinase, p38 α , and demonstrated that the η relaxation parameter is readily obtained to quantitatively measure the amplitude of the dynamics of the CF₃ moiety. In addition, the comparison of the FCT profile of the ligand in the non-deuterated receptor-bound state, relative to that of the perdeuterated receptor-bound state, indicated that the strategy would provide the surface complementarity information at the CF₃ site.

2. Results and Discussion

In the FCT analyses, the time (T)-dependent buildup of the intensity ratio of the multiple quantum coherence (I_{MQC}) over the single quantum coherence (I_{SQC}) is used to determine the motion- and distance-associated relaxation parameters η and δ , respectively, as following,

$$\frac{I_{MQC}}{I_{SQC}} = \frac{A\eta \cdot \tanh\left(\sqrt{\eta^2 + \delta^2}T\right)}{\sqrt{\eta^2 + \delta^2} - \delta \cdot \tanh\left(\sqrt{\eta^2 + \delta^2}T\right)} \quad (1)$$

where A is 0.5 and 0.75 for double and triple quantum coherence, respectively. Since the tetrahedral geometry and the rapid rotation around the threefold axis are common, the FCT analyses of both the CH_3 and CF_3 groups can be described by the same equation. Analogous to the FCT analyses for CH_3 groups [17], the equations defining the intra-trifluoromethyl ^{19}F - ^{19}F dipolar cross-correlated relaxation rate η_F and the heteronuclear dipolar cross relaxation of ^{19}F to external nuclei δ_F are described as below,

$$\eta_F = \frac{R_{2,F}^{fast} - R_{2,F}^{slow}}{2} \approx \frac{9}{10} [P_2(\cos\theta_{axis,FF})]^2 \frac{S_{axis}^2 \gamma_F^4 \hbar^2 \tau_C}{r_{FF}^6} \quad (2)$$

$$\delta_F = -4 \sum_{ext} \left(\frac{1}{20}\right) \frac{\hbar^2 \gamma_F^2 \gamma_X^2 \tau_C}{r_{FXext}^6} \quad (3)$$

where $R_{2,F}^{fast}$ and $R_{2,F}^{slow}$ are relaxation rates of fast and slow ^{19}F single quantum transitions, respectively. $P_2(x) = (1/2)(3x^2 - 1)$, $\theta_{axis,FF}$ is the angle between the trifluoromethyl threefold axis and the vector connecting two fluorine nuclei. S_{axis}^2 is the generalized order parameter, γ_F is the gyromagnetic ratio of F spins, γ_X is the gyromagnetic ratio of remote F or H spins, \hbar is the reduced Planck constant, τ_C is the rotational correlation time of the molecule, r_{FF} is the distance between two fluorine nuclei in a trifluoromethyl group, and r_{FXext} is the averaged distance between three fluorine atoms and an external H or F spin. Similar to that in the FCT analysis of a CH_3 group, the slope of the I_{MQC}/I_{SQC} buildup curve depends mostly on the η_F values. Therefore, the local dynamics of the ligand methyl groups in the ligand–receptor complex can be obtained from the initial CF_3 -FCT buildup. Analogously, the δ_F values, which reflect the vicinity of the CF_3 groups with external protons, i.e., surface complementarity, would be reflected in the plateau value of the I_{MQC}/I_{SQC} buildup.

However, some differences should be considered for assessing the practical applicability of the FCT analysis to the CF_3 groups. The smaller gyromagnetic ratio and the longer spin–spin distances in the CF_3 group, as compared to those in the CH_3 group, lead to smaller η and δ values in the CF_3 -FCT analyses. The gyromagnetic ratios for ^{19}F and ^1H are 251.662×10^6 rad/s/T and 267.513×10^6 rad/s/T, respectively. Interatomic ^{19}F - ^{19}F and ^1H - ^1H distances for the CF_3 and CH_3 groups are 2.164 Å and 1.813 Å, respectively. Assuming the same S_{axis}^2 and τ_C values, these differences make the η_F value 0.27-times smaller as compared to the η_H value. Therefore, the slope of the CF_3 -FCT buildup would be less steep, as compared to that of the CH_3 -FCT. This also means that the FCT profile of CF_3 requires a much longer mixing time to reach the plateau value, and thus, is less sensitive to the presence of external protons at practical mixing times, which are defined by the ^{19}F transverse relaxation times. In addition, the δ value itself tends to be smaller, as the van der Waals contact distance of fluorine is longer for a ^{19}F - ^1H pair (2.55 Å) as compared to that for a ^1H - ^1H pair (2.4 Å). At the van der Waals contact distance, the δ value is 0.61 times smaller for ^{19}F as compared to that for ^1H .

To experimentally evaluate the CF_3 -FCT analysis, we used p38 α , a 42 kDa mitogen-activated protein kinase, as a receptor. p38 α is a major drug target for inflammatory diseases such as rheumatoid arthritis and Crohn's disease [27,28]. For the ligand, we selected AST-487, which reportedly showed the highest p38 α -binding or inhibition potency among CF_3 -containing compounds in the ChEMBL Kinase SARfari database (Figure 1a) [29]. AST-487 was originally identified as a receptor tyrosine (RET) kinase inhibitor [30]. However, it is shown to bind also to p38 α with a dissociation constant (K_d) of 72 nM [31]. We verified the AST-487 binding to p38 α by an isothermal titration calorimetry (ITC) experiment, and observed a 1:1 exothermic interaction with a K_d value of 82.6 ± 13.5 nM (Figure 1b), which was identical to the reported value within the error. To further confirm that AST-487 binds to a specific site of p38 α , we carried out a chemical shift perturbation (CSP) experiment, in which AST-487 was titrated to p38 α with $^1\text{H}/^{13}\text{C}$ isotope labeling at the methyl positions of isoleucine ($\delta 1$),

leucine, valine, and methionine in a uniformly deuterated background ([ILVM-methyl- $^1\text{H}/^{13}\text{C}$, U- ^2H] p38 α) (Figure 2a and Supplementary Figure S1). Reflecting the high affinity of the complex, the ^1H - ^{13}C resonances of p38 α were perturbed in a slow exchange manner, saturating at one molar equivalent (Supplementary Figure S1). Methyl sites with substantial CSPs were mainly distributed in and near the ATP-binding site (Figure 2b), which is consistent with the canonical interaction mode of ATP-competitive inhibitors. In fact, intermolecular nuclear Overhauser effects (NOEs) were observed between the protons of AST-487 and the methyl protons in the ATP-binding site of p38 α (Figure 2c,d). Extensive NOEs were observed for the pyrimidine group and ether-linked ring of AST-487 (Figure 2c). In particular, NOEs were observed for the pyrimidine group and the p38 α methyl protons deeper in the ATP-binding cleft (orange spheres in Figure 2d). This NOE pattern is consistent with the binding mode of the AST-487-mitogen-activated protein kinase kinase 4 (MEK4) complex, which was previously analyzed by computational docking and saturation transfer difference (STD) NMR experiments, where the pyrimidine group of AST-487 resides deep in the binding cleft [32]. In contrast, we detected no intermolecular NOEs for the trifluoromethyl-phenyl ring and 4-ethyl-piperazin groups. This might be due to the lack of protons around these groups in the p38 α bound state, or to the less-efficient NOE transfer caused by fast local dynamics. Such an ambiguity can be clarified by quantifying the amplitude of the local dynamics. In addition, as described above, AST-487 binds a broad range of kinases including Tyr kinases (e.g., RET kinase) and Ser/Thr kinases (e.g., MEK4 and p38 α). Therefore, the dynamics information would contribute to the rational design of modifications for achieving better binding potency and the desired target specificity.

To characterize the dynamic property of the CF_3 group of AST-487 in the p38 α -bound state, we observed the ^{19}F resonance of the CF_3 moiety of AST-487 in the presence of p38 α . The ^{19}F resonance in the presence of p38 α was observed at -59.97 ppm, which was high field-shifted by 0.32 ppm from -59.65 ppm in the free state (Figure 3a). This resonance is derived from AST-487 in the bound state, as the binding of AST-487 to p38 α occurs in the slow exchange manner and saturates at one molar equivalent (Supplementary Figure S1). Then, we performed the double quantum coherence (DQC) and single quantum coherence (SQC) measurements of AST-487 complexed with perdeuterated p38 α . In these experiments, a broadband ^1H decoupling was applied throughout the pulse sequence to suppress the ^1H - ^{19}F scalar couplings. Mixing delays were set to 2.5, 5 and 7.5 ms, taking the signal decay due to the ^{19}F transverse relaxation into consideration (Supplementary Figure S2). Although no signal was observed in the DQC spectra of the free AST-487, the buildup of a DQC signal was clearly observed in a mixing time-dependent manner for AST-487 in the p38 α -bound state (Figure 3b). This supports that the signal observed in the p38 α -bound state is derived from the FCT phenomenon, which is allowed only under high-molecular-weight conditions. Thus, the results confirmed that the FCT measurement is applicable to the CF_3 group.

To estimate the motional amplitude of the CF_3 moiety, the I_{DQC}/I_{SQC} buildup was fitted to Equation 1 (Figure 3c). Here, we assumed $\delta_F = -28 \text{ s}^{-1}$, taking account of the intramolecular dipolar cross-relaxation from two adjacent protons at the van der Waals distance. The dipolar contribution from perdeuterated p38 α would be negligible. Under this assumption, the η_F value was determined as $18.3 \pm 1.96 \text{ s}^{-1}$. This corresponds to the Lipari-Szabo model-free S_{axis}^2 of 0.64 ± 0.069 . The estimated order parameter indicates that the CF_3 group and its directly attached phenyl ring of AST-487 retain a substantial mobility in the p38 α -bound state. This complements the lack of the NOE-based information about the intermolecular interaction for the trifluoromethyl-phenyl group.

We further investigated the effect of intermolecular dipole interactions on the CF_3 -FCT profile. To this end, we used non-deuterated p38 α , instead of perdeuterated p38 α , to introduce intermolecular dipole-dipole interactions between the CF_3 group of AST-487 and the protons of p38 α . The linewidth of the AST-487 ^{19}F resonance complexed with non-deuterated p38 α was broader than that with perdeuterated p38 α (102 and 72 Hz, respectively; Supplementary Figure S3a), indicating a considerable increase in dipole-dipole interactions. The I_{DQC}/I_{SQC} ratio of the CF_3 moiety at a mixing time of 5 ms was 24% smaller in the non-deuterated p38 α -bound state than that in the perdeuterated p38 α -bound

state (Supplementary Figure S3b). This could be ascribed to the enhancement of δ_F by the p38 α protons, indicating that the CF₃ group of AST-487 is at least partially buried in the binding pocket of p38 α . Thus, the result demonstrated that the surface complementarity information could be extracted from the CF₃-FCT analysis.

In summary, we demonstrated that the CF₃-FCT analyses are capable of characterizing the fast timescale motion and surface complementarity of the CF₃ group of a small ligand in the receptor-bound state. The extension of the FCT analyses to the CF₃ group would contribute to expanding the applicability of the dynamic SGDD to CF₃-containing molecules. The analyses provide important ways to proceed with the hit-to-lead and lead optimization processes to obtain a small compound with improved affinity and specificity for the drug-target biomolecules. Nevertheless, the utility of the CF₃-FCT analyses would not be limited to the field of drug development: the strategy might also be useful to characterize the functional dynamics of proteins. CF₃ groups have been chemically introduced to monitor the conformational equilibrium of proteins in structural analyses that are difficult to tackle by other methods [33–38].

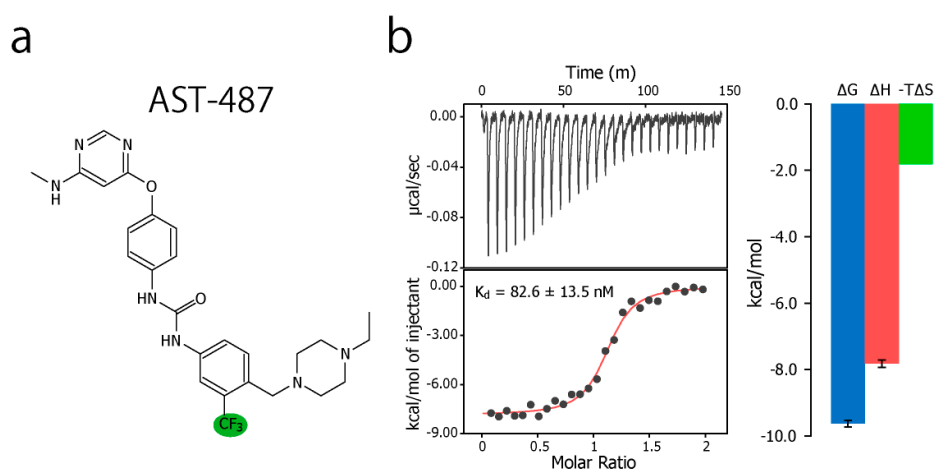


Figure 1. Chemical structure of AST-487 and its binding thermodynamics against p38 α . (a) The chemical structure of AST-487, with the CF₃ moiety highlighted in green; (b) The isothermal titration calorimetry (ITC) profile and thermodynamic properties of the interaction between AST-487 and p38 α . In the ITC experiment, 50 μ M AST-487 was titrated to 5 μ M p38 α at 25 $^{\circ}$ C.

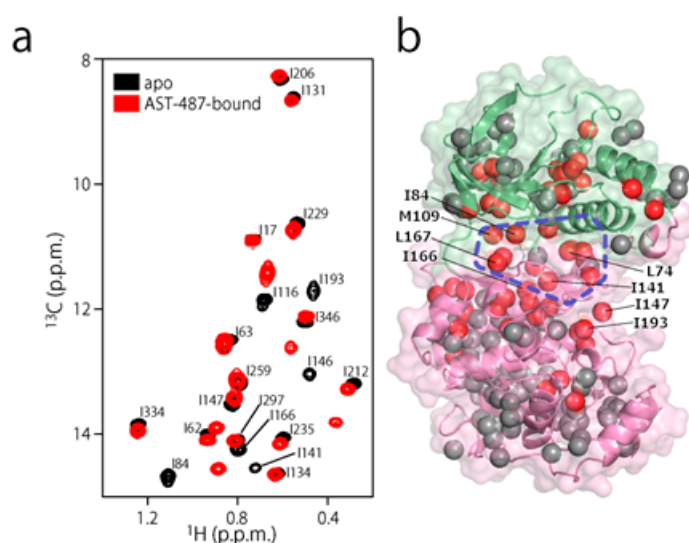


Figure 2. Cont.

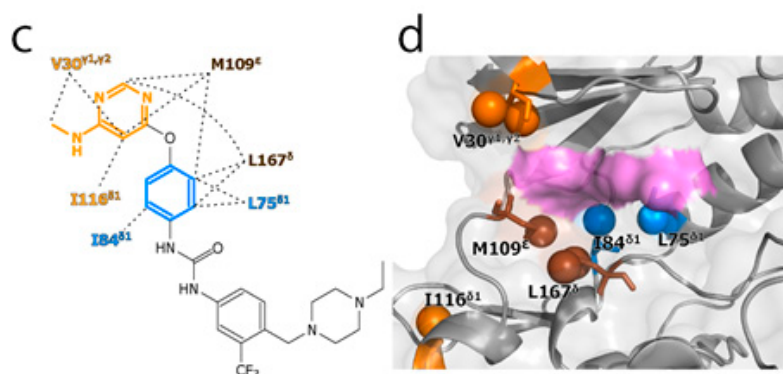


Figure 2. Structural characterization of the interaction between AST-487 and p38 α . (a) The ^1H - ^{13}C band-selective optimized-flip-angle short-transient-heteronuclear multiple quantum coherence (SOFAST-HMQC) spectra (Ile- $\delta 1$ region) of p38 α with $^1\text{H}/^{13}\text{C}$ isotope labeling at the methyl positions of isoleucine ($\delta 1$), leucine, valine, and methionine in a uniformly deuterated background ([ILVM-methyl- $^1\text{H}/^{13}\text{C}$, $\text{U-}^2\text{H}$] p38 α) in the presence (red) and absence (black) of an equimolar concentration of AST-487; (b) The structural mapping of the chemical shift perturbations (CSPs) induced by the addition of AST-487. Methyl groups with CSPs larger than the linewidth are shown as red spheres in the structure of p38 α in the apo state (Protein Data Bank (PDB) code: 1P38) [39]. The ATP-binding site is indicated by the blue broken line; (c) The intermolecular nuclear Overhauser effects (NOEs) observed between AST-487 and p38 α are illustrated by broken lines. For Leu-167, only one resonance of the two δ -methyl groups was identified with no stereospecific assignments; thus, it is labeled as “ δ ”. The pyrimidine ring and the methylamino substituent are colored orange, while the ether-linked phenyl ring is colored blue; (d) The methyl sites with intermolecular NOEs with AST-487 are shown as spheres in the p38 α structure (PDB code: 1A9U) [40]: orange methyl sites represent NOEs with the pyrimidine ring or its methylamino substituent; blue methyl sites represent NOEs with the ether-linked phenyl ring; and brown methyl sites represent NOEs to both. The surface of a representative p38 α inhibitor, SB203580, is colored purple to indicate the typical compound-binding site.

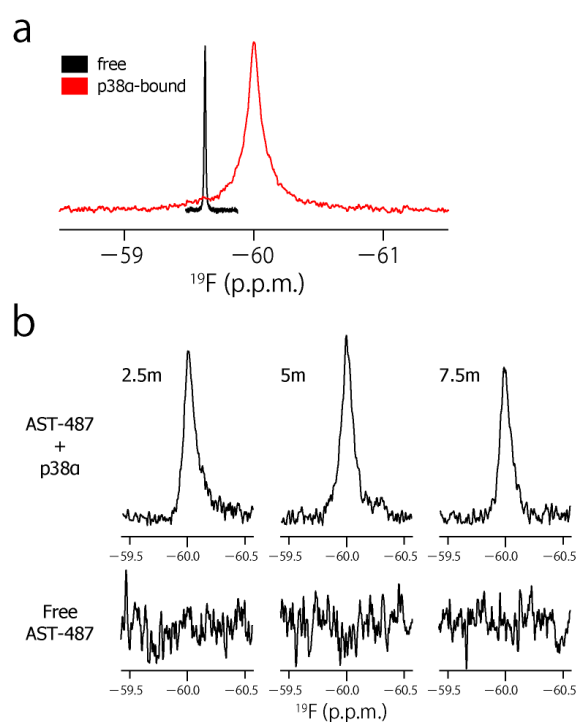


Figure 3. Cont.

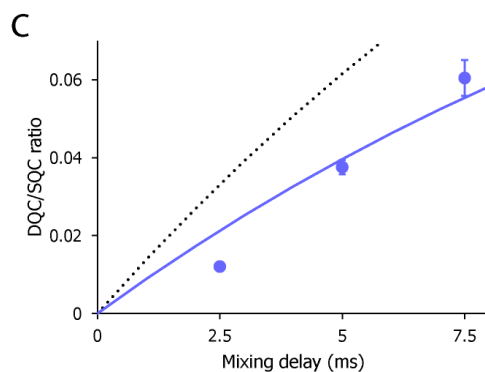


Figure 3. The CF_3 -FCT data of AST-487 complexed with p38 α . (a) Overlay of the ^{19}F -1D spectra of AST-487 in the presence (red) and absence (black) of perdeuterated p38 α ; (b) Spectral regions of the CF_3 resonance of AST-487 bound to perdeuterated p38 α (upper) and those in the absence of p38 α (lower) in the ^{19}F -DQC (double quantum coherence) spectra at mixing times of 2.5, 5 and 7.5 ms; (c) The time-dependent evolution of the $I_{\text{DQC}}/I_{\text{SQC}}$ ratio. Error bars are estimated from the signal-to-noise ratios. The fitting curve is drawn as a solid line. For comparison, a simulated curve with $S_{axis}^2 = 1$ ($\delta = -29 \text{ s}^{-1}$) is shown as a dotted line. SQC: single quantum coherence.

3. Materials and Methods

The compound AST-487 (molecular weight 529.6 Da, Purity 99.90%, Catalog No. SYN1210) was purchased from AK Scientific (Union City, CA, USA) and used without further purification. Powder of AST-487 was dissolved in $\text{DMSO-}(d_6)$ at a concentration of 100 mM, and small aliquots were stored at -30°C .

3.1. Preparation of the Recombinant p38 α

Overexpression and purification of the recombinant p38 α were performed following the procedure as reported previously [41]. Briefly, the *E. coli* strain BL21 (DE3) was transformed with the pET15b plasmid harboring an *N*-terminally hexahistidine-tagged human full-length p38 α sequence between the *Nco*I and *Xho*I restriction sites of the plasmid. Bacterial colonies grown on freshly prepared LB agar plates, containing 100 $\mu\text{g}/\text{mL}$ ampicillin, were inoculated into a 5 mL LB medium and cultured at 37°C overnight. For the production of perdeuterated p38 α , the overnight culture was mildly centrifuged and the resultant cell pellet was gently resuspended in a $100\times$ volume of D_2O -based M9 medium containing $^{15}\text{NH}_4\text{Cl}$ and $^2\text{H}_7\text{-D}$ -glucose as the sole nitrogen and carbon sources, respectively. When an optical density at 600 nm (OD_{600}) of 0.6 was reached, the culture temperature was lowered to 16°C . After 30 min, protein overexpression was induced by the addition of 0.6 mM isopropyl- β -D-thiogalactopyranoside (IPTG). For preparing $[\text{U-}^2\text{H}/^{15}\text{N}, \text{ILVM-methyl-}^1\text{H}/^{13}\text{C}]$ p38 α sample used in the p38 α -observed NMR experiment, methionine and precursors of isoleucine, leucine and valine were supplemented 30 min before induction at the following concentrations: 50 mg/L [ϵ - ^{13}C] l-methionine; 90 mg/L [3-methyl- ^{13}C , 3,4,4,4- D_4] α -ketoisovalerate, sodium salt; and 70 mg/L [methyl- ^{13}C , 3,3- D_2] α -ketobutyrate, sodium salt [42]. H_2O -based M9 medium with no isotope enrichment was used for the preparation of non-deuterated p38 α sample. Bacterial cells were collected by centrifugation and the cell pellet was stored at -80°C until purification. The cell suspension was sonicated on ice to lyse cells. The supernatant was subjected to metal-chelate affinity chromatography by using a His60 Ni Superflow column (Takara Bio, Shiga, Japan), followed by size-exclusion chromatography using a HiLoad 16/60 Superdex 200 prep grade column (GE Healthcare, Little Chalfont, UK). The elution fraction was concentrated in the buffered solution containing 25 mM Tris-HCl (pH 7.5), 150 mM NaCl and 5 mM dithiothreitol (DTT), by ultrafiltration using an Amicon Ultra centrifugal device (MWCO 10 kDa, 4 mL, Merck Millipore, Darmstadt, Germany). The concentration of p38 α was determined by measuring the ultraviolet absorbance at a wavelength of 280 nm and using an extinction coefficient of 47,850 L/mol/cm.

3.2. NMR Sample Preparation

All NMR samples were prepared in the buffered solution containing 25 mM Tris(D₁₁)-DCI (pH 7.7), 150 mM NaCl and 10 mM DTT-(D₁₀) in 95/5 D₂O/DMSO-(*d*₆). An aliquot of the p38 α stock in the H₂O-based buffer solution was buffer-exchanged to the DMSO-free NMR buffer by ultrafiltration using an Amicon Ultra device (MWCO 3 kDa, 0.5 mL). After adjusting the volume, the AST-487 solution and DMSO-(*d*₆) were added to have the final concentrations of 1 mM AST-487 and 5% (*v/v*) DMSO-(*d*₆). The concentrations of p38 α were 150 μ M and 400 μ M for p38 α -observed ¹H–¹³C correlation experiments and AST-487-observed ¹⁹F-detected experiments, respectively. To the latter samples, trifluoroacetic acid (TFA) was supplemented at a concentration of 500 μ M for chemical shift calibration.

3.3. NMR Experiments

Two dimensional ¹H–¹³C SOFAST-HMQC [43,44] spectra of p38 α in the absence and presence of AST-487 were acquired on a Bruker Avance 600 spectrometer equipped with a TXI cryoprobe operating at 298 K. The numbers of data points for the direct ¹H and the indirect ¹³C dimensions were 1024 and 512, with maximum acquisition times of 61.1 and 74.8 ms, respectively. Twelve transients were acquired per free induction decay (FID), with an interscan delay of 0.3 s. Time domain data were processed with TopSpin2.1 software (Bruker BioSpin, Billerica, MA, USA) and analyzed by Sparky [45]. Proton and carbon chemical shifts were calibrated using 4,4-dimethyl-4-silapentane-1-sulfonic acid (DSS) as the external standard [46]. Methyl sites experiencing CSPs larger than the linewidth upon AST-487 binding were classified as perturbed.

The rotational correlation time (τ_c) of p38 α was determined as 24 ns in 85/10/5 H₂O/D₂O/DMSO-based solution by transverse relaxation-optimized spectroscopy for rotational correlation times (TRACT) experiments [47]. Considering the increased viscosity due to higher D₂O content, the τ_c of p38 α in 95/5 D₂O/DMSO-based solutions used for FCT experiments was estimated to be 29 ns.

One-dimensional ¹⁹F-1D and the CF₃-FCT experiments were performed on a Bruker Avance 600 (Bruker BioSpin, Billerica, MA, USA) spectrometer equipped with a QCI-F cryoprobe at 298 K. The pulse sequence for the one-dimensional ¹⁹F-DQC and SQC experiments were analogous to those for proton DQC and SQC measurements, respectively [48]. The DQC and SQC experiments were performed with complex data points of 8096 and an acquisition time of 151 ms. For the DQC and SQC measurements, 46,080 and 1024 transients, respectively, were acquired with a recycling delay of 1.5 s. The mixing times were 2.5, 5.0 and 7.5 ms for experiments using perdeuterated p38 α , and 5 ms for those using non-deuterated p38 α . The ¹⁹F carrier frequency was set at –58.84 ppm. The WALTZ-16 composite pulse decoupling [49] was applied to proton spins from the excitation to the end of the acquisition period to suppress any potential ¹H–¹⁹F scalar couplings. The time domain data were processed and analyzed on the TopSpin3.1 software (Bruker Biospin), and the chemical shifts of ¹⁹F resonances were calibrated by using TFA as the internal standard.

3.4. ITC Experiments

The MicroCal VP-ITC calorimeter (Malvern, Malvern, UK) was used to determine the affinity and thermodynamic parameters associated with the binding of AST-487 to p38 α . AST-487 and p38 α were dissolved in the buffered solution (ITC buffer), containing 50 mM (*N*-2-hydroxyethylpiperazine-*N*-2-ethane sulfate (HEPES)–NaOH (pH 7.5), 150 mM NaCl, 1 mM tris(2-carboxyethyl)phosphine hydrochloride (TCEP), 4% (*v/v*) glycerol and 5% (*v/v*) DMSO. The ITC buffer was freshly prepared before use, passed through a 0.22- μ m membrane filter and degassed by sonication. The 100 mM stock of AST-487 was diluted 1:1000 with the ITC buffer and centrifuged. The resultant supernatant was filtered through a 0.22- μ m syringe filter. A stock solution of p38 α was exchanged to the ITC buffer by ultrafiltration using an Amicon Ultra (Merck Millipore, Darmstadt,

Germany) centrifugal device (MWCO 10 kDa) and filtered through a 0.22- μ m syringe filter. A total of 27 aliquots of 50 μ M AST-487 in the titration syringe (2 μ L at the initial titration point and 10 μ L at successive points) were added to the cell filled with 5 μ M p38 α , with an interval of 350 s between each pair of titration points at 25 °C. The reference titration data was acquired with the same titration procedure, except that the ITC buffer was used instead of the p38 α solution. After subtracting the reference data and omitting the initial titration point, the molar heat–ligand concentration profile was fitted to the one-to-one binding model by using the Origin software (OriginLab Corporation).

Supplementary Materials: Supplementary materials are available online. Figure S1: ATS-487 concentration-dependent spectral changes of p38 α , Figure S2: Estimation of the applicable mixing delays for CF₃–FCT analyses of the ATS-487-p38 α complex, and Figure S3: The effect of receptor protonation on the ¹⁹F linewidth and the FCT build up.

Acknowledgments: We thank Yu Tsutsumi (Bruker BioSpin) for the instructions for the ¹⁹F-NMR experiments. This work was supported by a grant from the Ministry of Economy, Trade, and Industry (METI) and Japan Agency of Medical Research and Development (AMED) to I.S. (Grant name: Development of core technologies for innovative drug development based upon IT). Funding was also provided by JST, PRESTO (Grant number JPMJPR14L5) to K.T., and by JSPS KAKENHI Grant Number 17K15083 to Y.T.

Author Contributions: Y.T., K.T. and I.S. conceived the project. Y.T. and K.T. performed the experiments. Y.T., K.T. and I.S. wrote the manuscript.

Conflicts of Interest: The authors declare no conflict of interest.

References

1. Klebe, G. Applying thermodynamic profiling in lead finding and optimization. *Nat. Rev. Drug Discov.* **2015**, *14*, 95–110. [[CrossRef](#)] [[PubMed](#)]
2. Tarcsay, Á.; Keserű, G.M. Is there a link between selectivity and binding thermodynamics profiles? *Drug Discov. Today* **2015**, *20*, 86–94. [[CrossRef](#)] [[PubMed](#)]
3. Ali, A.; Bandaranayake, R.M.; Cai, Y.; King, N.M.; Kolli, M.; Mittal, S.; Murzycki, J.F.; Nalam, M.N.; Nalivaika, E.A.; Ozen, A.; et al. Molecular basis for drug resistance in HIV-1 protease. *Viruses* **2010**, *2*, 2509–2535. [[CrossRef](#)] [[PubMed](#)]
4. Ohtaka, H.; Schön, A.; Freire, E. Multidrug resistance to HIV-1 protease inhibition requires cooperative coupling between distal mutations. *Biochemistry* **2003**, *42*, 13659–13666. [[CrossRef](#)] [[PubMed](#)]
5. Sheu, S.-Y.; Yang, D.-Y.; Selzle, H.L.; Schlag, E.W. Energetics of hydrogen bonds in peptides. *Proc. Natl. Acad. Sci. USA* **2003**, *100*, 12683–12687. [[CrossRef](#)] [[PubMed](#)]
6. Sheu, S.-Y.; Schlag, E.W.; Selzle, H.L.; Yang, D.-Y. Molecular dynamics of hydrogen bonds in protein—D₂O: The solvent isotope effect. *J. Phys. Chem. A* **2008**, *112*, 797–802. [[CrossRef](#)] [[PubMed](#)]
7. Rajeshwar, T.R.; Krishnan, M. Direct determination of site-specific noncovalent interaction strengths of proteins from NMR-derived fast side chain motional parameters. *J. Phys. Chem. B* **2017**, *121*, 5174–5186. [[CrossRef](#)] [[PubMed](#)]
8. Pellecchia, M.; Bertini, I.; Cowburn, D.; Dalvit, C.; Giralt, E.; Jahnke, W.; James, T.L.; Homans, S.W.; Kessler, H.; Luchinat, C.; et al. Perspectives on nmr in drug discovery: A technique comes of age. *Nat. Rev. Drug Discov.* **2008**, *7*, 738–745. [[CrossRef](#)] [[PubMed](#)]
9. Gossert, A.D.; Jahnke, W. NMR in drug discovery: A practical guide to identification and validation of ligands interacting with biological macromolecules. *Prog. Nucl. Magn. Reson. Spectrosc.* **2016**, *97*, 82–125. [[CrossRef](#)] [[PubMed](#)]
10. Lepre, C.A.; Moore, J.M.; Peng, J.W. Theory and applications of NMR-based screening in pharmaceutical research. *Chem. Rev.* **2004**, *104*, 3641–3676. [[CrossRef](#)] [[PubMed](#)]
11. Wand, A. Dynamic activation of protein function: A view emerging from NMR spectroscopy. *Nat. Struct. Biol.* **2001**, *8*, 926–931. [[CrossRef](#)] [[PubMed](#)]
12. Kay, L.E. New views of functionally dynamic proteins by solution nmr spectroscopy. *J. Mol. Biol.* **2016**, *428*, 323–331. [[CrossRef](#)] [[PubMed](#)]
13. Clore, G.M. Exploring sparsely populated states of macromolecules by diamagnetic and paramagnetic NMR relaxation. *Protein Sci.* **2011**, *20*, 229–246. [[CrossRef](#)] [[PubMed](#)]

14. Giovanni, L.; Attila, S. Model-free approach to the interpretation of nuclear magnetic resonance relaxation in macromolecules. 1. Theory and range of validity. *J. Am. Chem. Soc.* **1982**, *104*, 4546–4559.
15. Ban, D.; Sabo, T.M.; Griesinger, C.; Lee, D. Measuring dynamic and kinetic information in the previously inaccessible supra- τ (c) window of nanoseconds to microseconds by solution nmr spectroscopy. *Molecules* **2013**, *18*, 11904–11937. [[CrossRef](#)] [[PubMed](#)]
16. Sugase, K.; Dyson, H.J.; Wright, P.E. Mechanism of coupled folding and binding of an intrinsically disordered protein. *Nature* **2007**, *447*, 1021–1025. [[CrossRef](#)] [[PubMed](#)]
17. Tugarinov, V.; Sprangers, R.; Kay, L.E. Probing side-chain dynamics in the proteasome by relaxation violated coherence transfer nmr spectroscopy. *J. Am. Chem. Soc.* **2007**, *129*, 1743–1750. [[CrossRef](#)] [[PubMed](#)]
18. Mizukoshi, Y.; Takeuchi, K.; Arutaki, M.; Tokunaga, Y.; Takizawa, T.; Hanzawa, H.; Shimada, I. Improvement of ligand affinity and thermodynamic properties by NMR-based evaluation of local dynamics and surface complementarity in the receptor-bound state. *Angew. Chem. Int. Ed. Engl.* **2016**, *55*, 14606–14609. [[CrossRef](#)] [[PubMed](#)]
19. Wang, J.; Sánchez-Roselló, M.; Aceña, J.L.; del Pozo, C.; Sorochinsky, A.E.; Fustero, S.; Soloshonok, V.A.; Liu, H. Fluorine in pharmaceutical industry: Fluorine-containing drugs introduced to the market in the last decade (2001–2011). *Chem. Rev.* **2014**, *114*, 2432–2506. [[CrossRef](#)] [[PubMed](#)]
20. Furuya, T.; Kamlet, A.S.; Ritter, T. Catalysis for fluorination and trifluoromethylation. *Nature* **2011**, *473*, 470–477. [[CrossRef](#)] [[PubMed](#)]
21. Tomashenko, O.A.; Grushin, V.V. Aromatic trifluoromethylation with metal complexes. *Chem. Rev.* **2011**, *111*, 4475–4521. [[CrossRef](#)] [[PubMed](#)]
22. Gillis, E.P.; Eastman, K.J.; Hill, M.D.; Donnelly, D.J.; Meanwell, N.A. Applications of fluorine in medicinal chemistry. *J. Med. Chem.* **2015**, *58*, 8315–8359. [[CrossRef](#)] [[PubMed](#)]
23. Purser, S.; Moore, P.R.; Swallow, S.; Gouverneur, V. Fluorine in medicinal chemistry. *Chem. Soc. Rev.* **2008**, *37*, 320–330. [[CrossRef](#)] [[PubMed](#)]
24. Vulpetti, A.; Dalvit, C. Fluorine local environment: From screening to drug design. *Drug Discov. Today* **2012**, *17*, 890–897. [[CrossRef](#)] [[PubMed](#)]
25. Dalvit, C.; Ardini, E.; Fogliatto, G.P.; Mongelli, N.; Veronesi, M. Reliable high-throughput functional screening with 3-fabs. *Drug Discov. Today* **2004**, *9*, 595–602. [[CrossRef](#)]
26. Norton, R.S.; Leung, E.W.; Chandrashekar, I.R.; MacRaild, C.A. Applications of (^{19}F) -NMR in fragment-based drug discovery. *Molecules* **2016**, *21*, 860. [[CrossRef](#)] [[PubMed](#)]
27. Schindler, J.F.; Monahan, J.B.; Smith, W.G. P38 pathway kinases as anti-inflammatory drug targets. *J. Dent. Res.* **2007**, *86*, 800–811. [[CrossRef](#)] [[PubMed](#)]
28. Dodeller, F.; Schulze-Koops, H. The p38 mitogen-activated protein kinase signaling cascade in cd4 t cells. *Arthritis Res. Ther.* **2006**, *8*, 205. [[CrossRef](#)] [[PubMed](#)]
29. Bento, A.P.; Gaulton, A.; Hersey, A.; Bellis, L.J.; Chambers, J.; Davies, M.; Krüger, F.A.; Light, Y.; Mak, L.; McGlinchey, S.; et al. The chembl bioactivity database: An update. *Nucleic Acids Res.* **2014**, *42*, D1083–D1090. [[CrossRef](#)] [[PubMed](#)]
30. Akeno-Stuart, N.; Croyle, M.; Knauf, J.A.; Malaguarnera, R.; Vitagliano, D.; Santoro, M.; Stephan, C.; Grosios, K.; Wartmann, M.; Cozens, R.; et al. The ret kinase inhibitor NVP-ast487 blocks growth and calcitonin gene expression through distinct mechanisms in medullary thyroid cancer cells. *Cancer Res.* **2007**, *67*, 6956–6964. [[CrossRef](#)] [[PubMed](#)]
31. Davis, M.I.; Hunt, J.P.; Herrgard, S.; Ciceri, P.; Wodicka, L.M.; Pallares, G.; Hocker, M.; Treiber, D.K.; Zarrinkar, P.P. Comprehensive analysis of kinase inhibitor selectivity. *Nat. Biotechnol.* **2011**, *29*, 1046–1051. [[CrossRef](#)] [[PubMed](#)]
32. Deibler, K.K.; Mishra, R.K.; Clutter, M.R.; Antanasijevic, A.; Bergan, R.; Caffrey, M.; Scheidt, K.A. A chemical probe strategy for interrogating inhibitor selectivity across the mek kinase family. *ACS Chem. Biol.* **2017**, *12*, 1245–1256. [[CrossRef](#)] [[PubMed](#)]
33. Liu, J.J.; Horst, R.; Katritch, V.; Stevens, R.C.; Wüthrich, K. Biased signaling pathways in β 2-adrenergic receptor characterized by ^{19}F -NMR. *Science* **2012**, *335*, 1106–1110. [[CrossRef](#)] [[PubMed](#)]
34. Manglik, A.; Kim, T.H.; Masureel, M.; Altenbach, C.; Yang, Z.; Hilger, D.; Lerch, M.T.; Kobilka, T.S.; Thian, F.S.; Hubbell, W.L.; et al. Structural insights into the dynamic process of β 2-adrenergic receptor signaling. *Cell* **2015**, *161*, 1101–1111. [[CrossRef](#)] [[PubMed](#)]

35. Ye, L.; Van Eps, N.; Zimmer, M.; Ernst, O.P.; Prosser, R.S. Activation of the α_2 adenosine g-protein-coupled receptor by conformational selection. *Nature* **2016**, *533*, 265–268. [[CrossRef](#)] [[PubMed](#)]
36. Hattori, Y.; Heidenreich, D.; Ono, Y.; Sugiki, T.; Yokoyama, K.I.; Suzuki, E.I.; Fujiwara, T.; Kojima, C. Protein ^{19}F -labeling using transglutaminase for the nmr study of intermolecular interactions. *J. Biomol. NMR* **2017**. [[CrossRef](#)] [[PubMed](#)]
37. Prosser, R.S.; Kim, T.H. Nuts and bolts of CF_3 and CH_3 NMR toward the understanding of conformational exchange of GPCRs. *Methods Mol. Biol.* **2015**, *1335*, 39–51. [[PubMed](#)]
38. Didenko, T.; Liu, J.J.; Horst, R.; Stevens, R.C.; Wüthrich, K. Fluorine-19 NMR of integral membrane proteins illustrated with studies of gpcrs. *Curr. Opin. Struct. Biol.* **2013**, *23*, 740–747. [[CrossRef](#)] [[PubMed](#)]
39. Wang, Z.; Harkins, P.C.; Ulevitch, R.J.; Han, J.; Cobb, M.H.; Goldsmith, E.J. The structure of mitogen-activated protein kinase p38 at 2.1- \AA resolution. *Proc. Natl. Acad. Sci. USA* **1997**, *94*, 2327–2332. [[CrossRef](#)] [[PubMed](#)]
40. Wang, Z.; Canagarajah, B.J.; Boehm, J.C.; Kassisa, S.; Cobb, M.H.; Young, P.R.; Abdel-Meguid, S.; Adams, J.L.; Goldsmith, E.J. Structural basis of inhibitor selectivity in map kinases. *Structure* **1998**, *6*, 1117–1128. [[CrossRef](#)]
41. Tokunaga, Y.; Takeuchi, K.; Takahashi, H.; Shimada, I. Allosteric enhancement of map kinase p38 α 's activity and substrate selectivity by docking interactions. *Nat. Struct. Mol. Biol.* **2014**, *21*, 704–711. [[CrossRef](#)] [[PubMed](#)]
42. Goto, N.K.; Gardner, K.H.; Mueller, G.A.; Willis, R.C.; Kay, L.E. A robust and cost-effective method for the production of val, leu, ile (δ_1) methyl-protonated ^{15}N -, ^{13}C -, ^2H -labeled proteins. *J. Biomol. NMR* **1999**, *13*, 369–374. [[CrossRef](#)] [[PubMed](#)]
43. Schanda, P.; Kupce, E.; Brutscher, B. Sofast-HMQC experiments for recording two-dimensional heteronuclear correlation spectra of proteins within a few seconds. *J. Biomol. NMR* **2005**, *33*, 199–211. [[CrossRef](#)] [[PubMed](#)]
44. Amero, C.; Schanda, P.; Durá, M.A.; Ayala, I.; Marion, D.; Franzetti, B.; Brutscher, B.; Boisbouvier, J. Fast two-dimensional NMR spectroscopy of high molecular weight protein assemblies. *J. Am. Chem. Soc.* **2009**, *131*, 3448–3449. [[CrossRef](#)] [[PubMed](#)]
45. Goddard, T.D.; Keller, D.G. Sparky 3, University of California, San Francisco. Available online: <http://www.cgl.ucsf.edu/home/sparky/> (ver 3.114 distributed on 12th July 2007).
46. Harris, R.K.; Becker, E.D.; Cabral de Menezes, S.M.; Goodfellow, R.; Granger, P. NMR nomenclature: Nuclear spin properties and conventions for chemical shifts. Iupac recommendations 2001. *Solid State Nucl. Magn. Reson.* **2002**, *22*, 458–483. [[CrossRef](#)] [[PubMed](#)]
47. Lee, D.; Hilty, C.; Wider, G.; Wüthrich, K. Effective rotational correlation times of proteins from NMR relaxation interference. *J. Magn. Reson.* **2006**, *178*, 72–76. [[CrossRef](#)] [[PubMed](#)]
48. Kay, L.E.; Prestegard, J.H. Methyl group dynamics from relaxation of double quantum filtered NMR signals: Application to deoxycholate. *J. Am. Chem. Soc.* **1987**, *109*, 3829–3835. [[CrossRef](#)]
49. Shaka, A.J.; Keeler, J.; Frenkiel, T.; Freeman, R.A.Y. An improved sequence for broadband decoupling: Waltz-16. *J. Magn. Reson.* **1983**, *52*, 335–338. [[CrossRef](#)]

Sample Availability: Samples of the compound AST-487 (Purity 99.90%, Catalog No. SYN1210) is not available from the authors.



© 2017 by the authors. Licensee MDPI, Basel, Switzerland. This article is an open access article distributed under the terms and conditions of the Creative Commons Attribution (CC BY) license (<http://creativecommons.org/licenses/by/4.0/>).